HNPS Advances in Nuclear Physics

Vol 32 (2026)

HNPS2025

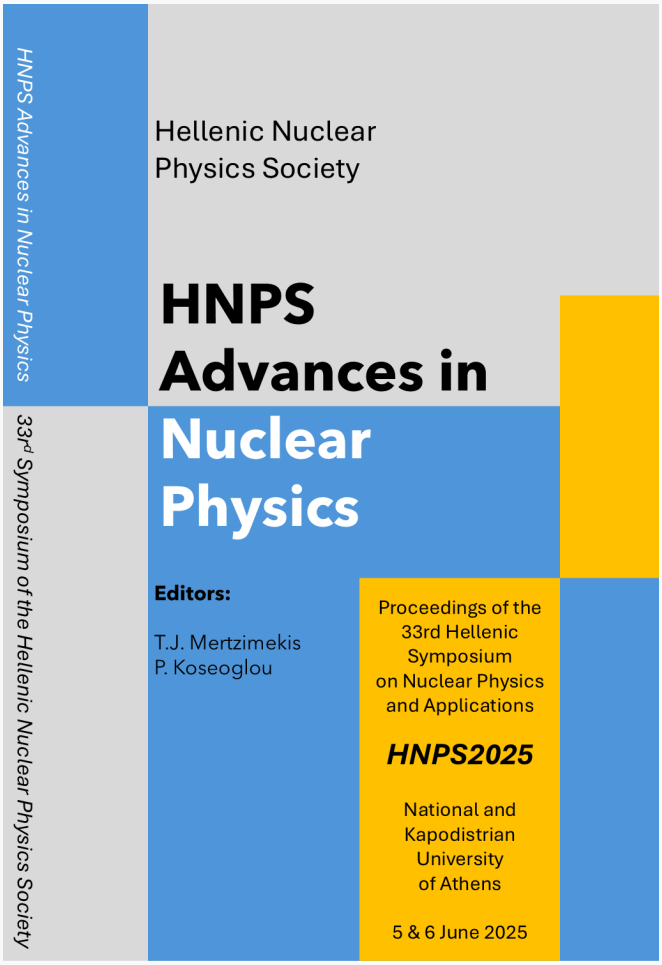

Nuclear Signatures and Stellar Observables: Bridging Terrestrial Experiments and Neutron Star Structure

Polychronis Koliogiannis Koutmiridis, Esra Yuksel, Tanmoy Ghosh, Nils Paar

doi: 10.12681/hnpsanp.8819

To cite this article:

Koliogiannis Koutmiridis, P., Yuksel, E., Ghosh, T., & Paar, N. (2026). Nuclear Signatures and Stellar Observables: Bridging Terrestrial Experiments and Neutron Star Structure. *HNPS Advances in Nuclear Physics*, *32*, 54–62. https://doi.org/10.12681/hnpsanp.8819

HNPS Advances in Nuclear Physics Vol. **32**, 54–62 (2025)
doi: 10.12681/hnpsanp.8819

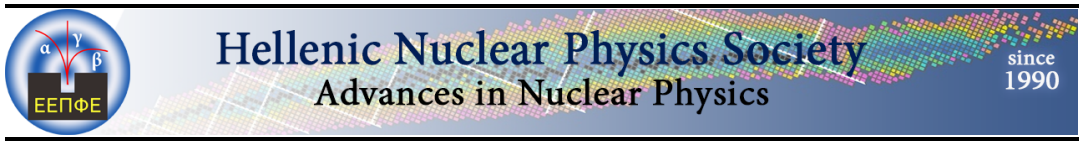

ARTICLE

Nuclear Signatures and Stellar Observables: Bridging Terrestrial Experiments and Neutron Star Structure

P.S. Koliogiannis,[*,1,2] E. Yüksel,[3] T. Ghosh,[1] and N. Paar[1]

[1]Department of Physics, Faculty of Science, University of Zagreb, Bijenička cesta 32, 10000, Zagreb, Croatia.
[2]Department of Theoretical Physics, Aristotle University of Thessaloniki, 54124, Thessaloniki, Greece.
[3]School of Mathematics and Physics, University of Surrey, Guildford, Surrey, GU2 7XH, United Kingdom.
*Corresponding author: pkoliogi@phy.hr

(Received: 06 Nov 2025; Accepted: 30 Nov 2025; Published: 01 Dec 2025)

Abstract

Insights into the properties of dense, neutron-rich matter emerge from the interplay between nuclear experiments and astrophysical observations. Measurements of parity-violating electron scattering on ^{48}Ca (CREX) and ^{208}Pb (PREX-2), together with electric dipole polarizability data, offer stringent probes of isovector dynamics in nuclei. In this study, a set of relativistic energy density functionals is employed to investigate how these nuclear signatures correlate with neutron star observables, such as stellar radii and tidal deformabilities. By confronting the theoretical predictions with data from both terrestrial experiments and multimessenger observations—including the gravitational wave event GW170817—constraints are derived on the symmetry energy and the high-density behavior of the equation of state. The analysis highlights the influence of including the fourth-order term in the isospin-asymmetry expansion of the energy density on neutron star radius and tidal deformability predictions. At the same time, discrepancies between constraints from CREX and PREX-2 underscore the need for improved experimental precision and additional astrophysical input to refine our understanding of dense matter.

Keywords: Neutron stars; Gravitational waves; Equation of state; Relativistic energy density functional; Parity-violating electron scattering

1. Introduction

A detailed understanding of neutron star physics relies on the knowledge of the equation of state (EoS) of nuclear matter, which governs the relation between pressure and energy density and, consequently, stellar structure. Despite major progress, the density dependence of the nuclear symmetry energy—particularly above nuclear saturation density—remains one of the main uncertainties in modern nuclear astrophysics. These ambiguities directly affect the EoS and in turn influence theoretical predictions of neutron star characteristics. More precisely, the symmetry energy has a dual significance in nuclear and astrophysical domains: it contributes to the isovector channel of the nuclear interaction, shaping the behavior of finite nuclei, while simultaneously acting as a key

 ISBN 2654-007X (print), 2654-0088 (online).

component in the EoS of neutron-rich stellar matter, thereby impacting macroscopic observables. Consequently, the symmetry energy represents a crucial link between nuclear experiments and astrophysical observations, bridging the fields of nuclear physics and neutron star astrophysics [1–3].

Considerable effort has been devoted to exploring the symmetry energy and its slope around nuclear saturation density, as well as to establishing correlations with various nuclear observables, including weak form factors and neutron skin thickness [4–8]. Particularly relevant are recent parity-violating electron scattering measurements from the CREX (^{48}Ca) [9] and PREX-2 (^{208}Pb) [10] experiments, which offer direct insights into these quantities. At higher densities, complementary constraints are provided by astrophysical data, since the symmetry energy governs several aspects of neutron star physics—its composition, thermal evolution, crustal properties, and radius [3]. Binary merger events, most notably GW170817 [11], have further restricted the low- and intermediate-density regimes of the EoS through precise measurements of tidal deformability and stellar radii. Recent studies [12–17] have pursued a unified approach, combining laboratory and astrophysical data to constrain the density dependence of the symmetry energy and its impact on compact star observables.

In the present study, we employ a series of β-equilibrated EoSs for neutron-star matter, constructed using relativistic energy density functionals (EDFs) with density-dependent point-coupling (DD-PC) interactions [17], along with additional EoSs adjusted to reproduce the recent CREX and PREX-2 measurements [18]. The EDF framework provides a consistent description of both finite nuclei and neutron stars, thereby enabling a direct connection between experimental observables—such as weak form factors and neutron skin thickness—and macroscopic stellar quantities, including the radius and tidal deformability of a 1.4 $M_\odot$ neutron star. Through this unified approach, new constraints on the dense-matter EoS are derived. A comprehensive account of the analysis and results is given in Ref. [19]; the present work summarizes the key findings and their relevance for ongoing efforts to bridge nuclear and astrophysical constraints.

The manuscript is structured as follows. Section 2 outlines the theoretical framework and the employed EoS models. The results and their discussion are presented in Section 3, while concluding remarks are summarized in Section 4.

2. Framework and Models

The present analysis integrates a family of eight DD-PC functionals, labeled DD-PC-J29…36 [17]. These functionals were developed within the relativistic EDF framework and optimized to reproduce ground-state nuclear properties, while systematically varying the symmetry energy at saturation between $J = 29$ and 36 MeV. A detailed discussion of their construction can be found in Ref. [19] and references therein. In addition, the DD-PC-CREX, DD-PC-PREX, DD-PC-REX, and DD-PCX functionals [20] were employed. The first three incorporate constraints from weak form factor measurements in the CREX and PREX-2 experiments, while DD-PCX was calibrated using both isovector dipole and isoscalar monopole excitation properties of ^{208}Pb, alongside with nuclear ground-state data. This comprehensive set of EDFs enables a systematic exploration of the nuclear symmetry energy and its influence on dense-matter properties.

Based on these microscopic nuclear interactions, the nuclear framework was extended to the astrophysical domain for the description of neutron stars. In particular, the stellar medium was modeled as charge-neutral, β-equilibrated $npe\mu$ matter. The corresponding baryonic energy density and pressure are expressed as

$$\mathcal{E}_b(\rho,\delta) = \rho E_b(\rho,\delta), \quad \text{and} \quad P_b(\rho,\delta) = \rho^2 \frac{\partial E_b(\rho,\delta)}{\partial \rho}, \tag{1}$$

where $E_b(\rho,\delta)$ denotes the energy per baryon, which can be expanded in powers of the isospin asymmetry parameter $\delta = (\rho_n - \rho_p)/(\rho_n + \rho_p)$ as

$$E_b(\rho,\delta) = E_b(\rho,0) + \sum_{k=2,4} \delta^k S_k(\rho), \quad \text{with} \quad S_k(\rho) = \frac{1}{k!}\frac{\partial^k E_b(\rho,\delta)}{\partial \delta^k}\Big|_{\delta=0}, \tag{2}$$

and $E_b(\rho,0)$ being the energy per baryon of symmetric nuclear matter. When the leptonic contributions, treated as a relativistic Fermi gas, are included, β-equilibrated EoSs are obtained: (a) a family of DD-PC EoSs for which the symmetry energy was systematically varied ($J = 29$–36 MeV); (b) two DD-PC EoSs calibrated to CREX and PREX-2 measurements, respectively; (c) one DD-PC EoS constrained by the combination of CREX and PREX-2 experiments; and (d) one DD-PC EoS constrained by dipole polarizability data.

Afterward, the macroscopic structure of neutron stars is determined by solving the Tolman–Oppenheimer–Volkoff equations,

$$\frac{dP(r)}{dr} = -\frac{G\mathcal{E}(r)M(r)}{c^2 r^2}\left(1+\frac{P(r)}{\mathcal{E}(r)}\right)\left(1+\frac{4\pi P(r) r^3}{M(r)c^2}\right)\left(1-\frac{2GM(r)}{c^2 r}\right)^{-1}, \tag{3}$$

$$\frac{dM(r)}{dr} = \frac{4\pi r^2}{c^2}\mathcal{E}(r), \tag{4}$$

which are solved self-consistently with the underlying EoS, yielding the pressure and enclosed mass as functions of radius r, thus providing fundamental properties of neutron stars.

In addition, information from gravitational-wave observations constrains the low-density regime of the EoS through the effective tidal deformability $\tilde{\Lambda}$, defined for a binary system as

$$\tilde{\Lambda} = \frac{16}{13}\frac{(12q+1)\Lambda_1 + (12+q)q^4\Lambda_2}{(1+q)^5}, \tag{5}$$

where $q = m_2/m_1 \leq 1$ denotes the binary mass ratio and Λ_i represents the dimensionless tidal deformability of the i-th component,

$$\Lambda_i = \frac{2}{3}k_2\left(\frac{R_i c^2}{M_i G}\right)^5 \equiv \frac{2}{3}k_2\beta_i^{-5}, \quad i = 1,2, \tag{6}$$

with k_2 being the tidal Love number, $\beta = GM/(Rc^2)$ the compactness, and M_i, R_i the mass and radius of each star. Since Λ_i is strongly dependent on R_i, the tidal deformability serves as a sensitive probe connecting the microscopic nuclear properties with macroscopic neutron star observables. For the crustal region, the following EoSs were adopted: the Baym–Pethick–Sutherland EoS [21] for the outer crust, the Feynman–Metropolis–Teller EoS [22] at lower densities, and the SLy EoS [23] for the inner crust, up to the crust–core transition density $\rho_{\rm tr}$ [23]. The transition density is determined via the thermodynamical method [24], ensuring a consistent matching between the crust and core regions.

3. Results and Discussion

The structure of neutron stars, obtained from the DD-PC EoSs, is presented in detail in Fig. 1(a) through the corresponding mass–radius dependencies. In particular, solid curves correspond to the family of DD-PC EoSs, where the symmetry energy varies in the range $J = 29, 30, \ldots, 36$ MeV, with darker colors denoting higher values of symmetry energy, while dashed, dash-dotted, dotted, and dash-dot-dotted curves denote the DD-PC-CREX, DD-PC-PREX, DD-PC-REX, and DD-PCX EoSs,

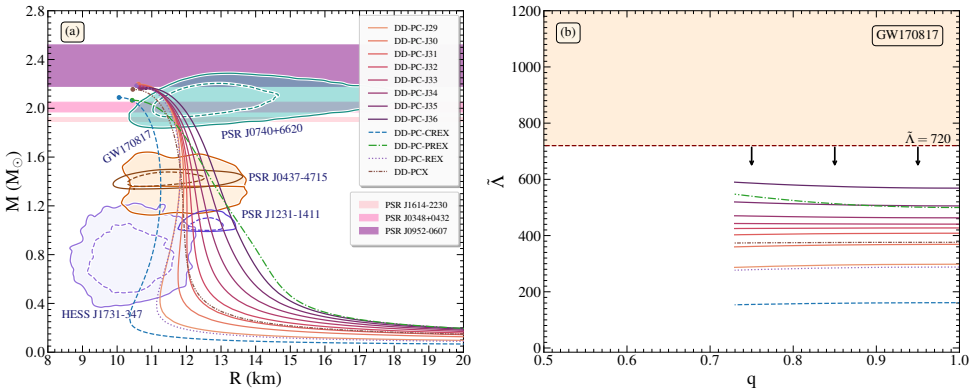

Figure 1. (a) Gravitational mass as a function of the radius for the DD-PC EoSs. The solid lines denote the family of DD-PC EoSs spanning $J = 29, 30, ..., 36$ MeV, while the dashed, dash-dotted, dotted, and dash-dot-dotted lines correspond to the DD-PC-CREX, DD-PC-PREX, DD-PC-REX, and DD-PCX EoSs, respectively. The shaded contours from bottom to top represent the HESS J1731-347 remnant [25], the PSR J1231-1411 [26], the PSR J0437-4715 [27], the GW170817 event [11], and the PSR J0740+6620 [28, 29], while the horizontal shaded regions denote the PSR J1614-2230 [30], PSR J0348+0432 [31], and PSR J0952-0607 [32] pulsar observations with possible maximum neutron star mass. (b) The corresponding effective tidal deformability as a function of the binary mass ratio. The shaded region represents the excluded values provided by LIGO for the GW170817 event [11].

respectively. The figure also includes recent astrophysical constraints from pulsar measurements, covering both maximum mass and radius determinations, as well as data from the binary merger event GW170817 [11, 25–32]. In this context, all considered EoSs satisfy the observational bounds on mass and radius, while the softer models with lower symmetry energy ($J = 29$–32 MeV) are additionally compatible with the ultra-light compact remnant HESS J1731–347 [25]. Complementary, Fig. 1(b) shows the effective tidal deformability $\tilde{\Lambda}$ as a function of the binary mass ratio, indicating that the predicted values also fall within the limits set by the GW170817 analysis.

In the following, the analysis addresses the correlations between nuclear and astrophysical observables. Figure 2 shows the dimensionless tidal deformability at 1.4 $M_\odot$, $\Lambda_{1.4}$, as a function of the charge–weak form factor difference $F_{ch} - F_w$ and the neutron skin thickness R_{np} for both ^{48}Ca and ^{208}Pb. In detail, the DD-PC family is represented by crosses, with darker colors corresponding to higher J values; DD-PC-CREX by pentagon, DD-PC-PREX by up-triangle, DD-PC-REX by down-triangle, and DD-PCX by star. In all cases, an exponential dependence emerges, with the DD-PC family forming a well-defined correlation, while larger deviations appear for the rest models, specifically those constrained by CREX and PREX-2.

In addition, the shaded bands in Fig. 2 represent nuclear and astrophysical constraints, whose overlap defines the subset of EoSs consistent with both nuclear observables under consideration: charge-weak form factor and neutron skin thickness. This consistency is expected given the strong correlation between charge–weak form factor and neutron skin thickness. From an astrophysical point of view, all EoSs comply with the GW170817 tidal deformability bounds. However, on the nuclear physics side, CREX results favor EoSs with a smaller symmetry energy, while PREX-2 supports stiffer EoSs with $J \gtrsim 35$ MeV. This discrepancy manifests in the CREX- and PREX-2–adjusted functionals (DD-PC-CREX and DD-PC-PREX), which bracket the behavior of the DD-PC family. A similar pattern is observed in Fig. 3, which displays the radius at 1.4 $M_\odot$, $R_{1.4}$, as a function of $F_{ch} - F_w$ and R_{np} for both nuclei.

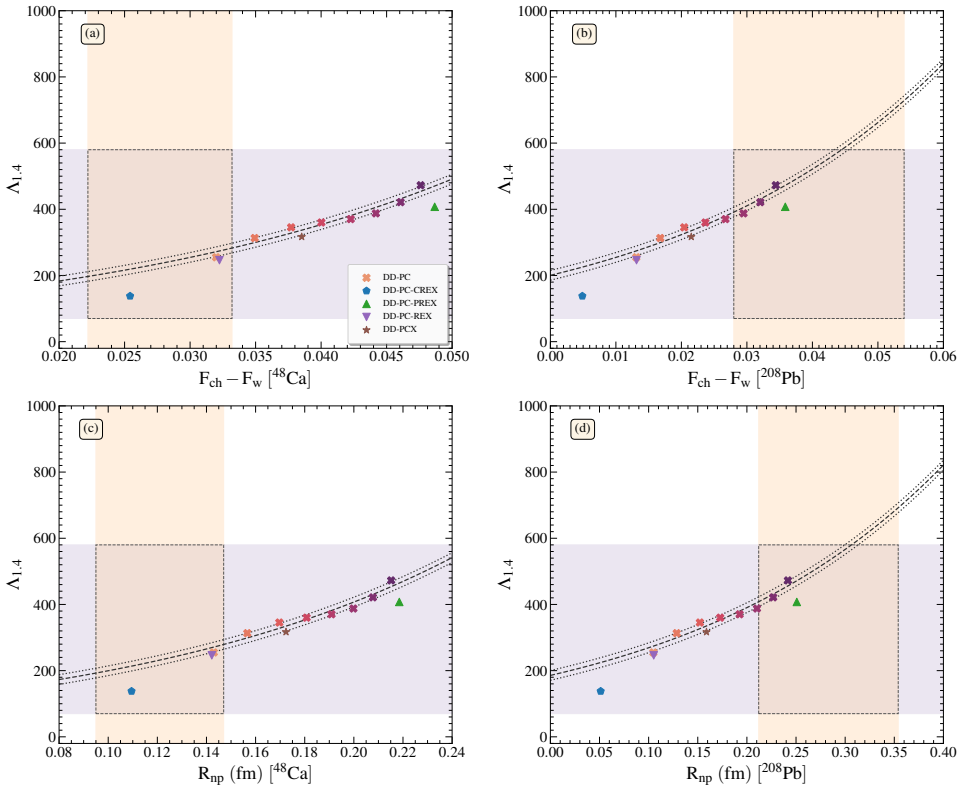

Figure 2. Dimensionless tidal deformability at $1.4\ M_\odot$ as a function of (a,b) the difference between charge and weak form factors and (c,d) the neutron skin thickness for ^{48}Ca (left panel) and ^{208}Pb (right panel) nuclei. The horizontal shaded region represents the constraints from GW170817 event [11], while the vertical shaded regions correspond to the experimental constraints extracted from (a,c) CREX and (b,d) PREX-2. The symbols denote different EoSs: DD-PC family of EoSs (crosses, where darker color denotes higher values of J), DD-PC-CREX (pentagon), DD-PC-PREX (up-triangle), DD-PC-REX (down-triangle), and DD-PCX (star). The dashed line represents the fit corresponding to the DD-PC family of EoSs, while the dotted lines denote the standard deviation.

These correlations are quantified using an exponential relation of the form

$$Q = c_1 \exp(c_2 \mathcal{N}) + c_3, \tag{7}$$

where Q represents either $\Lambda_{1.4}$ or $R_{1.4}$, and $\mathcal{N}$ corresponds to $F_{\rm ch} - F_{\rm w}$ or $R_{\rm np}$. The fitted parameters, corresponding standard deviations, and coefficients of determination are summarized in Table 1. In Figs. 2 and 3, the exponential relation (7) is shown as a dashed line, while the associated standard deviation is indicated by a dotted line. These relations enable the translation of nuclear measurements into neutron star constraints, including the radius and the symmetry energy: (a) CREX corresponds to $R_{1.4} \in [11.790, 11.861]$ km and $J \in [24.306, 29.037]$ MeV, while (b) PREX-2 favors $R_{1.4} \geq 12.417$ km and $J \geq 34.190$ MeV, yielding an offset of about 0.5 km between the two radius predictions [19].

Accounting for the intrinsic correlation between radius and tidal deformability, an additional empirical relation, $\Lambda_{1.4} = c_4 R_{1.4}^{c_5}$, with coefficients $c_4 = 5.389 \times 10^{-4}$ and $c_5 = 5.357$ ($r = 0.957$, $R^2 = 0.897$), was employed to characterize the general behavior of DD-PC EoSs, as shown in Fig. 4. By imposing the GW170817 upper bound on $\Lambda_{1.4}$, the stellar radius is limited to $R_{1.4} \leq 13.366$ km—consistent with previous determinations. This range also overlaps with that inferred from PREX-2, implying an upper limit on the symmetry energy at saturation of $J \leq 36.658$ MeV. Although CREX and PREX-2

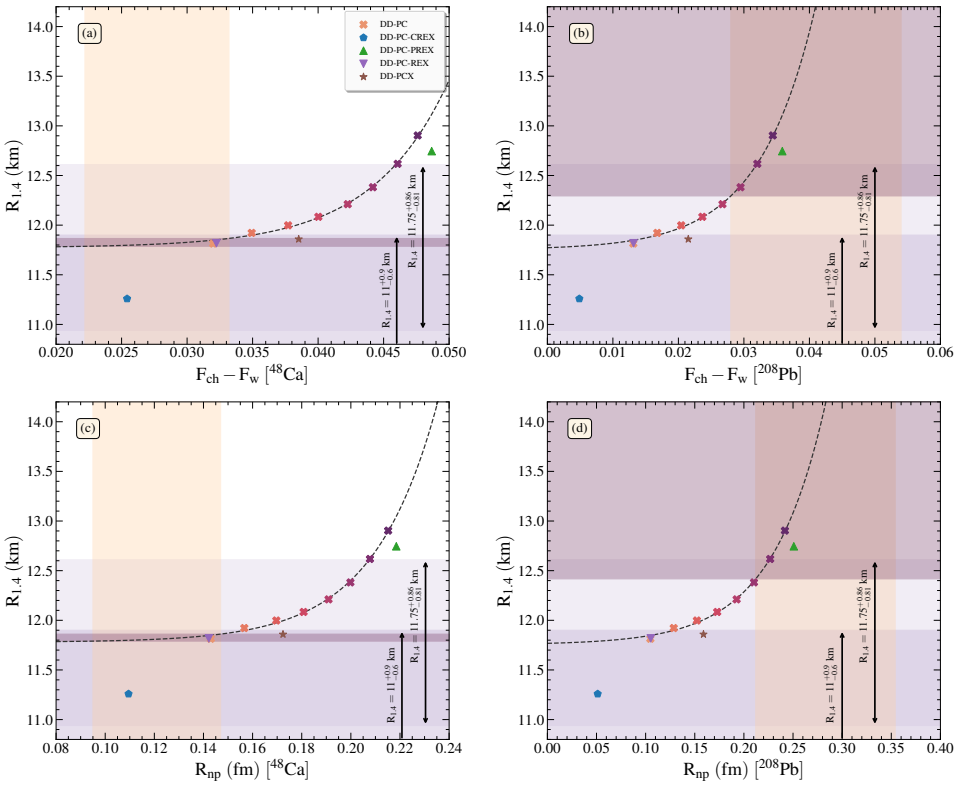

Figure 3. Radius at $1.4\,M_\odot$ as a function of (a,b) the difference between charge and weak form factors and (c,d) neutron skin thickness for the ^{48}Ca (left panel) and ^{208}Pb (right panel) nuclei. The vertical shaded region represents the experimental constraints extracted from (a,c) CREX and (b,d) PREX-2, while the horizontal shaded regions correspond to constraints extracted from Refs. [33, 34]. The symbols denote different EoSs: DD-PC family of EoSs (crosses, where darker color denotes higher values of J), DD-PC-CREX (pentagon), DD-PC-PREX (up-triangle), DD-PC-REX (down-triangle), and DD-PCX (star). The dashed line represents the fit corresponding to the DD-PC family of EoSs (since $\sigma \ll 0.1$, the standard deviation is not plotted).

Table 1. Coefficients of expression (7) for ^{48}Ca and ^{208}Pb nuclei for $Q = \Lambda_{1.4}$, $R_{1.4}$, and $\mathcal{N} = F_{\rm ch} - F_{\rm w}$, $R_{\rm np}$. In addition, the standard deviation, σ, and the coefficient of determination R^2 are also noted. The units of coefficients and σ are defined so $\Lambda_{1.4}$ and $F_{\rm ch} - F_{\rm w}$ to be dimensionless, $R_{1.4}$ to be in km, and $R_{\rm np}$ to be in fm.

	Nuclei	$\mathcal{N}$	c_1	c_2	c_3	σ	R^2
$\Lambda_{1.4}$	^{48}Ca	$F_{\rm ch} - F_{\rm w}$	94.946	32.874	–	14.611	0.944
		$R_{\rm np}$	97.846	7.129	–	14.674	0.944
	^{208}Pb	$F_{\rm ch} - F_{\rm w}$	200.443	23.895	–	14.768	0.943
		$R_{\rm np}$	185.554	3.719	–	14.751	0.943
$R_{1.4}$	^{48}Ca	$F_{\rm ch} - F_{\rm w}$	3.084×10^{-4}	172.174	11.772	0.019	0.997
		$R_{\rm np}$	2.931×10^{-4}	38.317	11.779	0.019	0.997
	^{208}Pb	$F_{\rm ch} - F_{\rm w}$	2.068×10^{-2}	116.622	11.752	0.018	0.997
		$R_{\rm np}$	1.374×10^{-2}	18.282	11.754	0.018	0.997

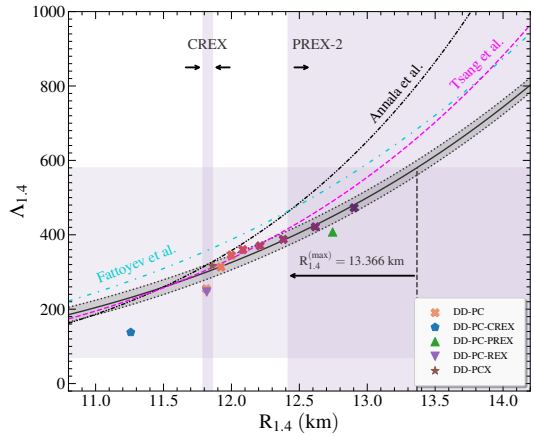

Figure 4. Dimensionless tidal deformability as a function of the radius at $1.4\,M_\odot$ for the DD-PC EoSs. The horizontal shaded region represents the GW170817 event [11], while the vertical shaded regions correspond to the constraints derived in this work [19]. The grey solid line represents the fit for the DD-PC family of EoSs, with the dotted lines denoting the standard deviation. Additional comparisons include expressions from Refs. [35–37].

provide uncertainties of similar magnitude, their implications diverge: CREX supports smaller J values and narrower radius intervals associated with the flatter portion of the exponential trend, whereas PREX-2 points to larger J values and broader radius variations along the steeper section of the relation.

4. Conclusion

In this study, the interplay between nuclear observables and neutron star properties has been examined within the framework of relativistic EDFs. Incorporating a set of EoSs derived from DD-PC interactions—along with modified versions adjusted to the CREX and PREX-2 data—we have analyzed how weak form factor and neutron skin thickness measurements can constrain the nuclear symmetry energy and, consequently, the radius and tidal deformability of neutron stars. Our results reaffirm the overall consistency of the DD-PC models with previous findings, while also revealing the distinct implications of the two recent experiments: CREX favors a softer symmetry energy at saturation, whereas PREX-2 suggests a stiffer behavior. Through empirical correlations between finite-nucleus observables and neutron star parameters, we obtained corresponding bounds on $R_{1.4}$ and J. Remarkably, the DD-PC-REX EoS follows closely the systematic trend of the DD-PC family, producing values of $R_{1.4}$ and J that fall within the CREX-compatible range.

Future high-precision experiments and astrophysical observations, particularly from next-generation gravitational-wave detectors and improved parity-violating electron scattering measurements, are expected to further tighten existing constraints. These advances will help achieve a more unified and quantitative understanding of dense matter, reinforcing the connection between nuclear structure and neutron star astrophysics.

Acknowledgments

This work is supported by the Croatian Science Foundation under the project number HRZZ-MOBDOL-12-2023-6026 and under the project Relativistic Nuclear Many-Body Theory in the Multimessenger Observation Era (HRZZ-IP-2022-10-7773). This work was supported by the project “Implementation of cutting-edge research and its application as part of the Scientific Center of Excellence for

Quantum and Complex Systems, and Representations of Lie Algebras“, Grant No. PK.1.1.10.0004, co-financed by the European Union through the European Regional Development Fund - Competitiveness and Cohesion Programme 2021-2027. E.Y. acknowledges support from the UK STFC under award no. ST/Y000358/1.

References

[1] A.W. Steiner, M. Prakash, J.M. Lattimer, and P.J. Ellis. “Isospin asymmetry in nuclei and neutron stars”. In: *Phys. Rep.* 411.6 (2005), pp. 325–375. ISSN: 0370-1573. DOI: 10.1016/j.physrep.2005.02.004.

[2] G.F. Burgio and I. Vidaña. “The Equation of State of Nuclear Matter: From Finite Nuclei to Neutron Stars”. In: *Universe* 6.8 (2020). ISSN: 2218-1997. DOI: 10.3390/universe6080119.

[3] J.M. Lattimer. “Constraints on Nuclear Symmetry Energy Parameters”. In: *Particles* 6.1 (2023), pp. 30–56. ISSN: 2571-712X. DOI: 10.3390/particles6010003.

[4] X. Roca-Maza and N. Paar. “Nuclear equation of state from ground and collective excited state properties of nuclei”. In: *Prog. Part. Nucl. Phys.* 101 (2018), pp. 96–176. ISSN: 0146-6410. DOI: 10.1016/j.ppnp.2018.04.001.

[5] C. Mondal, B.K. Agrawal, M. Centelles, G. Colò, X. Roca-Maza, N. Paar, X. Viñas, S.K. Singh, and S.K. Patra. “Model dependence of the neutron-skin thickness on the symmetry energy”. In: *Phys. Rev. C* 93 (6 2016), p. 064303. DOI: 10.1103/PhysRevC.93.064303.

[6] X. Roca-Maza, M. Brenna, G. Colò, M. Centelles, X. Viñas, B.K. Agrawal, N. Paar, D. Vretenar, and J. Piekarewicz. “Electric dipole polarizability in ^{208}Pb: Insights from the droplet model”. In: *Phys. Rev. C* 88 (2 2013), p. 024316. DOI: 10.1103/PhysRevC.88.024316.

[7] X. Roca-Maza, X. Viñas, M. Centelles, B.K. Agrawal, G. Colò, N. Paar, J. Piekarewicz, and D. Vretenar. “Neutron skin thickness from the measured electric dipole polarizability in ^{68}Ni, ^{120}Sn, and ^{208}Pb”. In: *Phys. Rev. C* 92 (6 2015), p. 064304. DOI: 10.1103/PhysRevC.92.064304.

[8] P.-G. Reinhard, J. Piekarewicz, W. Nazarewicz, B.K. Agrawal, N. Paar, and X. Roca-Maza. “Information content of the weak-charge form factor”. In: *Phys. Rev. C* 88 (3 2013), p. 034325. DOI: 10.1103/PhysRevC.88.034325.

[9] D. Adhikari et al. “Precision Determination of the Neutral Weak Form Factor of ^{48}Ca”. In: *Phys. Rev. Lett.* 129 (4 2022), p. 042501. DOI: 10.1103/PhysRevLett.129.042501.

[10] D. Adhikari et al. “Accurate Determination of the Neutron Skin Thickness of ^{208}Pb through Parity-Violation in Electron Scattering”. In: *Phys. Rev. Lett.* 126 (17 2021), p. 172502. DOI: 10.1103/PhysRevLett.126.172502.

[11] B.P. Abbott et al. “Properties of the Binary Neutron Star Merger GW170817”. In: *Phys. Rev. X* 9 (1 2019), p. 011001. DOI: 10.1103/PhysRevX.9.011001.

[12] T.-G. Yue, L.-W. Chen, Z. Zhang, and Y. Zhou. “Constraints on the symmetry energy from PREX-II in the multimessenger era”. In: *Phys. Rev. Res.* 4 (2 2022), p. L022054. DOI: 10.1103/PhysRevResearch.4.L022054.

[13] R. Essick, I. Tews, P. Landry, and A. Schwenk. “Astrophysical Constraints on the Symmetry Energy and the Neutron Skin of ^{208}Pb with Minimal Modeling Assumptions”. In: *Phys. Rev. Lett.* 127 (19 2021), p. 192701. DOI: 10.1103/PhysRevLett.127.192701.

[14] R. Essick, P. Landry, A. Schwenk, and I. Tews. “Detailed examination of astrophysical constraints on the symmetry energy and the neutron skin of ^{208}Pb with minimal modeling assumptions”. In: *Phys. Rev. C* 104 (6 2021), p. 065804. DOI: 10.1103/PhysRevC.104.065804.

[15] B.T. Reed, F.J. Fattoyev, C.J. Horowitz, and J. Piekarewicz. “Implications of PREX-2 on the Equation of State of Neutron-Rich Matter”. In: *Phys. Rev. Lett.* 126 (17 2021), p. 172503. DOI: 10.1103/PhysRevLett.126.172503.

[16] B. Biswas. “Impact of PREX-II and Combined Radio/NICER/XMM-Newton’s Mass–radius Measurement of PSR J0740+6620 on the Dense-matter Equation of State”. In: *Astrophys. J.* 921.1 (2021), p. 63. DOI: 10.3847/1538-4357/ac1c72.

[17] E. Yüksel, T. Oishi, and N. Paar. “Nuclear Equation of State in the Relativistic Point-Coupling Model Constrained by Excitations in Finite Nuclei”. In: *Universe* 7.3 (2021). ISSN: 2218-1997. DOI: 10.3390/universe7030071.

[18] E. Yüksel and N. Paar. “Implications of parity-violating electron scattering experiments on ^{48}Ca (CREX) and ^{208}Pb (PREX-II) for nuclear energy density functionals”. In: *Phys. Lett. B* 836 (2023), p. 137622. ISSN: 0370-2693. DOI: 10.1016/j.physletb.2022.137622.

[19] P.S. Koliogiannis, E. Yüksel, and N. Paar. “Constraining neutron star properties through parity-violating electron scattering experiments and relativistic point coupling interactions”. In: *Phys. Lett. B* 862 (2025), p. 139362. ISSN: 0370-2693. DOI: 10.1016/j.physletb.2025.139362.

[20] E. Yüksel, T. Marketin, and N. Paar. “Optimizing the relativistic energy density functional with nuclear ground state and collective excitation properties”. In: *Phys. Rev. C* 99 (3 2019), p. 034318. DOI: 10.1103/PhysRevC.99.034318.

[21] G. Baym, C. Pethick, and P. Sutherland. “The Ground State of Matter at High Densities: Equation of State and Stellar Models”. In: *Astrophys. J.* 170 (1971), p. 299. DOI: 10.1086/151216.

[22] R.P. Feynman, N. Metropolis, and E. Teller. “Equations of State of Elements Based on the Generalized Fermi-Thomas Theory”. In: *Phys. Rev.* 75 (10 1949), pp. 1561–1573. DOI: 10.1103/PhysRev.75.1561.

[23] F. Douchin and P. Haensel. “A unified equation of state of dense matter and neutron star structure”. In: *Astron. Astrophys.* 380.1 (2001), pp. 151–167. DOI: 10.1051/0004-6361:20011402.

[24] N. Paar, Ch.C. Moustakidis, T. Marketin, D. Vretenar, and G.A. Lalazissis. “Neutron star structure and collective excitations of finite nuclei”. In: *Phys. Rev. C* 90 (1 2014), p. 011304. DOI: 10.1103/PhysRevC.90.011304.

[25] V. Doroshenko, V. Suleimanov, G. Pühlhofer, and A. Santangelo. “A strangely light neutron star within a supernova remnant.” In: *Nat. Astron.* 6 (12 2022), 1444–1451. DOI: 10.1038/s41550-022-01800-1.

[26] T. Salmi et al. “A NICER View of PSR J1231-1411: A Complex Case”. In: *Astrophys. J.* 976.1 (2024), p. 58. DOI: 10.3847/1538-4357/ad81d2.

[27] D. Choudhury et al. “A NICER View of the Nearest and Brightest Millisecond Pulsar: PSR J0437–4715”. In: *Astrophys. J. Lett.* 971.1 (2024), p. L20. DOI: 10.3847/2041-8213/ad5a6f.

[28] E. Fonseca et al. “Refined Mass and Geometric Measurements of the High-mass PSR J0740+6620”. In: *Astrophysical J. Lett.* 915.1 (2021), p. L12. DOI: 10.3847/2041-8213/ac03b8.

[29] A.J. Dittmann et al. “A More Precise Measurement of the Radius of PSR J0740+6620 Using Updated NICER Data”. In: *Astrophysical J.* 974.2 (2024), p. 295. DOI: 10.3847/1538-4357/ad5f1e.

[30] Z. Arzoumanian et al. “The NANOGrav 11-year Data Set: High-precision Timing of 45 Millisecond Pulsars”. In: *Astrophys. J. Suppl. S.* 235.2 (2018), p. 37. DOI: 10.3847/1538-4365/aab5b0.

[31] J. Antoniadis et al. “A Massive Pulsar in a Compact Relativistic Binary”. In: *Sci.* 340.6131 (2013), p. 1233232. DOI: 10.1126/science.1233232.

[32] R.W. Romani, D. Kandel, A.V. Filippenko, T.G. Brink, and W. Zheng. “PSR J0952-0607: The Fastest and Heaviest Known Galactic Neutron Star”. In: *Astrophys. J. Lett.* 934.2 (2022), p. L17. DOI: 10.3847/2041-8213/ac8007.

[33] C.D. Capano, I. Tews, S.M. Brown, B. Margalit, S. De, S. Kumar, D.A. Brown, B. Krishnan, and S. Reddy. “Stringent constraints on neutron-star radii from multimessenger observations and nuclear theory”. In: *Nat. Astron.* 4 (6 2020), pp. 625–632. DOI: 10.1038/s41550-020-1014-6.

[34] T. Dietrich, M.W. Coughlin, P.T.H. Pang, M. Bulla, J. Heinzel, L. Issa, I. Tews, and S. Antier. "Multimessenger constraints on the neutron-star equation of state and the Hubble constant". In: *Sci.* 370.6523 (2020), pp. 1450–1453. DOI: 10.1126/science.abb4317.

[35] E. Annala, T. Gorda, A. Kurkela, and A. Vuorinen. "Gravitational-Wave Constraints on the Neutron-Star-Matter Equation of State". In: *Phys. Rev. Lett.* 120 (17 2018), p. 172703. DOI: 10.1103/PhysRevLett.120.172703.

[36] F.J. Fattoyev, J. Piekarewicz, and C.J. Horowitz. "Neutron Skins and Neutron Stars in the Multimessenger Era". In: *Phys. Rev. Lett.* 120 (17 2018), p. 172702. DOI: 10.1103/PhysRevLett.120.172702.

[37] C.Y. Tsang, M.B. Tsang, P. Danielewicz, F.J. Fattoyev, and W.G. Lynch. "Insights on Skyrme parameters from GW170817". In: *Phys. Lett. B* 796 (2019), pp. 1–5. ISSN: 0370-2693. DOI: 10.1016/j.physletb.2019.05.055.